**Thomas Léonard**
SAFRAN – Turbomeca,
DT/MD/MO,
Bordes Cedex 1 64511, France

**Laurent Y. M. Gicquel**
CERFACS,
Computational Fluid Dynamics Team,
42 Avenue G. Coriolis,
Toulouse Cedex 1 31057, France

**Nicolas Gourdain**
CERFACS,
Computational Fluid Dynamics Team,
42 Avenue G. Coriolis,
Toulouse Cedex 1 31057, France

**Florent Duchaine**[1]
CERFACS,
Computational Fluid Dynamics Team,
42 Avenue G. Coriolis,
Toulouse Cedex 1 31057, France
e-mail: florent.duchaine@cerfacs.fr

# Steady/Unsteady Reynolds-Averaged Navier–Stokes and Large Eddy Simulations of a Turbine Blade at High Subsonic Outlet Mach Number

*Reynolds-averaged Navier–Stokes (RANS), unsteady RANS (URANS), and large eddy simulation (LES) numerical approaches are clear candidates for the understanding of turbine blade flows. For such blades, the flow unsteady nature appears critical in certain situations and URANS or LES should provide more physical understanding as illustrated here for a laboratory high outlet subsonic Mach blade specifically designed to ease numerical validation. Although RANS offers good estimates of the mean isentropic Mach number and boundary layer thickness, LES and URANS are the only approaches that reproduce the trailing edge flow. URANS predicts the mean trailing edge wake but only LES offers a detailed view of the flow. Indeed, LESs identify flow phenomena in agreement with the experiment, with sound waves emitted from the trailing edge separation point that propagate upstream and interact with the lower blade suction side.*
[DOI: 10.1115/1.4028493]

## Introduction

Recent advances in computing power allow new strategies to be considered for the understanding of turbine blade flows. Among the potential numerical methods, three approaches are of clear interest to industry. The RANS model is the most common and theoretically mature method. Indeed, RANS benefits from an extensive industrial use and numerous turbulent flow models specifically derived for wall bounded flows [1,2]. Note that RANS as introduced initially by Reynolds [3] (i.e., based on a statistical mean solution of the turbulent Navier–Stokes equations) is theoretically restrained to stationary flows. The URANS approach offers a revised model of RANS to address potentially nonstationary and unsteady flows [4]. LES is an alternative to URANS. In this approach, the notion of scale separation is introduced by explicitly or implicitly spatially filtering out the small, more universal, turbulent flow scales from the large unsteady flow motions [5,6]. With all approaches, turbulent models are required. While RANS and URANS benefit from high order turbulent models and tuned wall models [7], LES relies on the more classical mixing length turbulent model [6]. Wall models are scarce and specific developments are still being pursued [8].

In the context of turbine blades, where the unsteady nature of the turbulent flow appears critical, URANS and LES are good candidates and should provide more physical understanding of the key physics. To illustrate the potential of these approaches, the laboratory turbine blade configuration of Sieverding et al. [9,10] is first simulated by use of RANS, URANS, and LES. The fully structured numerical approach is first used for all computations with specifically refined wall regions. All three results are gauged against experimental findings [9,10] not only in the mean sense but also for unsteady features. To further investigate the LES approach, comparisons and grid dependencies of the results are then presented for fully structured and unstructured simulations.

In the first part of this work, the target configuration is detailed along with the computational models, RANS, URANS, and LES. The computational domain and set of boundary conditions used for the structured mesh comparisons are detailed prior to a discussion on the flow features as obtained by the three modeling methods. All results presented in this first part of the work are gauged against experimental measurements. The second part concentrates on the LES approach. Implicit as well as explicit time integration schemes are investigated in the context of different grid resolutions and topologies: two fully structured meshes and three fully unstructured meshes. The aim of this last section is to discuss the differences in numerical strategies and the impact they may have on the LES flow dynamics which is further to be validated against flow temporal records.

## Target Configuration

The test configuration comes from the work of Sieverding et al. [9,10], which is the outcome of the European Research Project BRITE/EURAM CT96-0143 on "Turbulence Modeling of Unsteady Flows in Axial Turbines." The design of the blade (Fig. 1(*a*)) is targeted to allow the diagnostic of the trailing edge vortex shedding on the steady and unsteady trailing blade pressure distribution of a laboratory turbine blade at high subsonic Mach number ($M_{2\mathrm{is}} = 0.79$) and high Reynolds number ($\mathrm{Re}_2 = 2{,}800{,}000$, based on the chord and outlet velocity). The configuration is adapted to preserve the 2D flow as much as possible. The vortex formation and shedding process are visualized using high speed schlieren camera and a holographic interferometric density measuring technique. A cascade of five blades composes the experimental setup. The central blade is equipped with a rotatable trailing edge cylinder instrumented side-by-side with a pressure tap and a fast response pressure sensor for detailed

[1]Corresponding author.

Contributed by the International Gas Turbine Institute (IGTI) of ASME for publication in the Journal of Turbomachinery. Manuscript received October 12, 2010; final manuscript received August 26, 2014; published online October 28, 2014. Assoc. Editor: Beth Wisler.

  

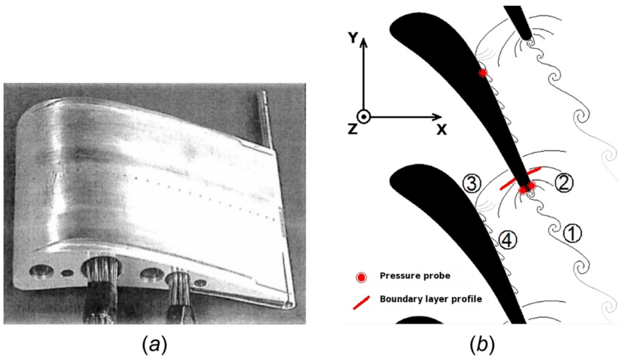


**Fig. 1 Blade design (*a*) as experimentally studied by Refs. [9] and [10] and (*b*) expected flow features and available measurement stations [9,10]**

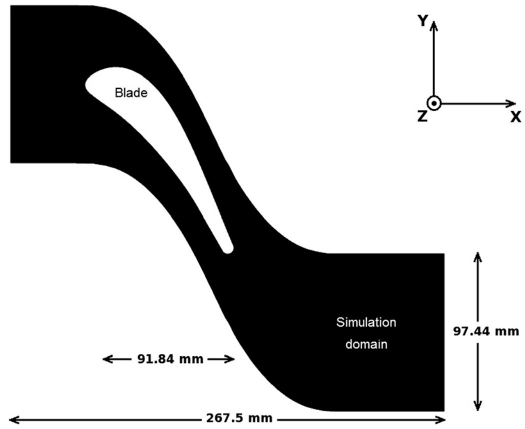


**Fig. 3 Computational domain retained for all RANS, URANS, and LES predictions**

measurements of the trailing edge pressure distribution. To complement the data, isentropic Mach distributions are provided along the suction and pressure side of the blade as well as boundary layer velocity profiles at two stations (Fig. 1(*b*)). Finally, pressure variations are recorded experimentally at several locations within the flow to allow for unsteady quantification of the phenomena involved.

Based on these detailed measurements, four unsteady flow features are identified as critical in determining the mean flow field of such a turbine blade. The leading flow structure, denoted by 1 in Fig. 1(*b*), is the vortex shedding issued by the blade trailing edge boundary layer separation. Associated to this separation point is the generation of pressure wave (denoted by 2 in Fig. 1(*b*)) traveling upstream. These waves then eventually interact with the lower blade suction side (3) to produce skin vortices (4), which then travel in the downstream direction along the blade wall. All details on the diagnostics and specificities of the experimental setup are not detailed here but can be found in Refs. [9] and [10].

## Modeling Strategies: RANS, URANS, and LES

Application of the direct numerical simulations to turbine blade flows is still unpractical because of the flow Reynolds number [6,11]. Modeling is thus a prerequisite and different turbulence modeling formulations are available [5,6,11,12] to mimic the cascade of turbulence over a wide range of applications with high Reynolds numbers. At the same time, supercomputers have reached peak performances and memory increases allow full three-dimensional simulations of real experimental and industrial configurations to be considered [13,14]. These applications still remain limited to the RANS formulation where all of the turbulent effects on the mean flow are provided by the model (Fig. 2(*a*)). Extension of the approach to treat unsteady flows, with periodic and nonturbulent flow structures, provides a new level of description as recently demonstrated by the use of URANS [4]. The alternative to RANS or URANS which are derived from a statistical ensemble of flow states may be modeled by turbulent scale separation as introduced by LES. With this formulation, only one flow state is considered and the behavior of the large turbulent structures which evolve in time and space are explicitly computed by the filtered Navier–Stokes equations (Fig. 2(*b*)). This separation of scales is explicitly or implicitly obtained by filtering out the small flow scales that cannot be properly represented on the mesh [5,6], their effect on the filtered field being modeled by the so-called subgrid-scale (SGS) model (Fig. 2(*b*)).

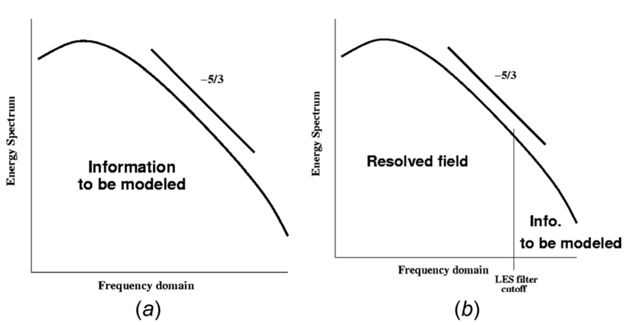


**Fig. 2 Conceptual representation of the turbulent information to be supplied in (*a*) RANS or URANS and (*b*) LES in the context of a turbulent isotropic flow**

Although all three approaches have advantages and trade-offs, the gain obtained by increasing the level of description of the flow represented by the unsteady compressible Navier–Stokes equations is not clear from an industrial point of view. Unsteadiness is known to be of importance in turbine flows [13–16]. However, the computing cost issued by going from RANS to URANS and then LES still requires justification from a scientific standpoint. As a preliminary answer to such issues, the three levels of computational descriptions are provided for the Sieverding et al. [9,10] blade row for which detailed diagnostics have been gathered on mean flow quantities as well as time series to characterize the large structure unsteadiness.

**Numerical Parameterization.** In order to proceed with the computation of the Sieverding configuration, a 3D computational domain corresponding to a single blade channel is chosen (Fig. 3). The characteristic dimensions of the domain are provided in Fig. 3 along with the typical blade dimensions given in Table 1. Note that top, bottom, and side boundaries of the computational domain are assumed periodic in agreement with the experimental findings. Inlet and outlet flow boundaries are positioned far enough from the profile to limit their impact on the predictions: i.e., respectively located 0.5 $c_{ax}$ upstream the leading edge and 1.5 $c_{ax}$ downstream the trailing edge.[2] Finally, a no-slip adiabatic wall condition is applied at the blade surface. Details on the quantities prescribed and the type of boundary condition used are summarized in Table 2.

The initial set of numerical predictions are obtained by use of the same fully structured mesh presented in Fig. 4 and which is composed of 500,000 hexahedra distributed around the blade in five block-structured domains with coincident interfaces except at the periodic boundary conditions which are noncoincident and are treated through a no-match condition. The numerical scheme is

[2]Sensitivity to the exit boundary condition treatment and relative position from the blade trailing edge has been specifically studied. The current results provide the best solution as discussed in a dedicated article under review.

**Table 1 Blade cascade characteristic dimensions**

| | |
|---|---|
| Chord length | 140 mm |
| Axial chord length | 0.656 |
| Pitch to chord ratio | 0.696 |
| Blade height | 100 mm |
| Aspect ratio | 0.714 |
| Trailing edge thickness to chord ratio | 0.0531 |
| Trailing edge wedge angle | 7.5 deg |
| Inlet angle (from axial direction) | 0 deg |
| Gauging angle | 70.9 deg |
| Stagger angle | 49.83 deg |
| Number of blades | 4 |

**Table 2 Boundary conditions as used in all computations**

| Boundary condition | Flow quantity imposed | Values |
|---|---|---|
| Inlet | Total pressure | 140,000 Pa |
| | Total temperature | 280 K |
| | Flow angle | 0 deg |
| Outlet | Pressure | 92,755 Pa |
| Blade wall | No-slip adiabatic wall | — |
| Top | Periodicity | — |
| Bottom | Periodicity | — |
| Front | Periodicity | — |
| Back | Periodicity | — |

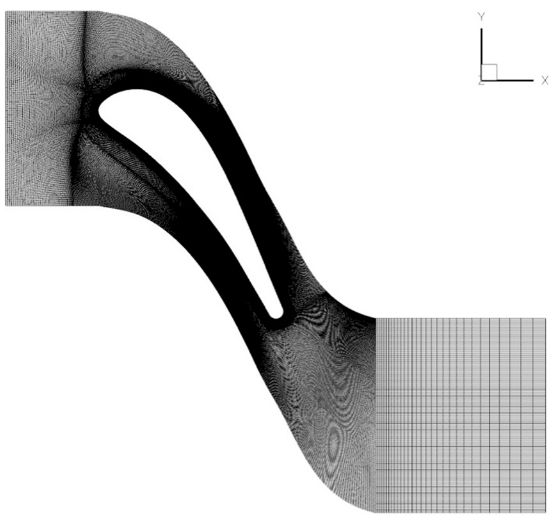


**Fig. 4 Typical mesh topology used for RANS, URANS, and LES**

second order in space and relies on an implicit integration based on a finite-volume approach. Turbulent closure relies for RANS and URANS on the classical $k$–$\omega$ model [17] with no specific treatment at the wall other than the limiting procedure proposed by Zheng et al. [18]. Indeed, with the grid generated here, typical mean $y^+$ of the first flow cells of the wall are estimated at five guaranteeing reasonable quality boundary layer estimates provided that the turbulent model behaves adequately in these regions of the flow.[3] LES and URANS computations use a fixed time-step ($\Delta t = 1.56 \times 10^{-7}$ s or an acoustic CFL (Courant, Friedrichs, and Lewy number) condition of 0.7). Time marching for the structured code relies on the dual time-stepping approach [19] while the unstructured code uses an explicit third order accurate scheme

[3]Without points inside the viscous sublayer (i.e., $y^+ < 1$) and without appropriate functions, the k–$\omega$ turbulence model cannot be guaranteed to predict the isentropic Mach number.

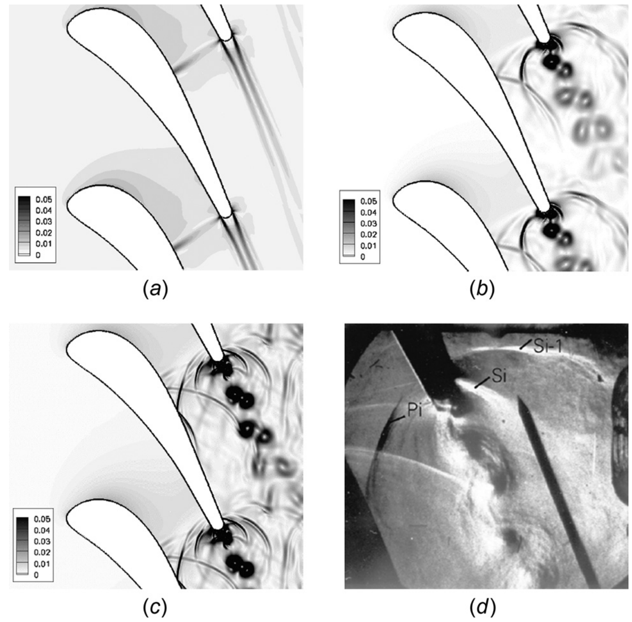


**Fig. 5 Norm of the density gradient as obtained by use of (*a*) RANS, (*b*) URANS, (*c*) LES at given instants, and (*d*) a direct view at the trailing edge flow dynamics as seen in the experiment [9,10]**

[20]. SGS closure is obtained for all cases by use of the Smagorinsky model [21] with constant at 0.09 as recommended for wall bounded applications [22–24] and without damping function.

**RANS, URANS, and LES Validations.** A typical view of the flow quantities, here the norm of the density gradient, is illustrated in Fig. 5 for (*a*) RANS, (*b*) URANS, and (*c*) LES. To complement the view, a snapshot of the experiment focusing on the trailing edge region of the flow is provided in Fig. 5(*d*). All three numerical formulations result in distinct flow behaviors. RANS provides a mean temporal view of the flow field for the configuration under investigation. With this approach (Fig. 5(*a*)), the local flow acceleration issued by the suction side flow passage restriction is clearly visible and induces a region of density gradient in the upstream part of the suction side. After the blade throat, a density gradient appears indicating the potential presence of a weak shock. The higher density gradients appear on each side of the trailing edge and are linked with the wake region induced by the blade boundary layer separations at the end of the blade and the boundary layer itself. The time dependent description of the flow (URANS) provides new insights on the mean periodic solution (Fig. 5(*b*)). With this approach, the local flow acceleration in the upstream region seems reduced if compared to RANS. The weak shock at the throat is no longer present. At the trailing edge and instead of a mixed out wake, vortex shedding appears along with a network of interacting density fronts (pressure waves in fact). Two distinct sets of waves are identified in agreement with Sieverding et al. [9,10] and denoted in Fig. 5(*d*) by $S_i$ and $P_i$, respectively. Both sets of waves originate from the boundary layer separation point on the suction and pressure sides of the blade trailing edge. In URANS, the suction side generated pressure waves, $S_i$, propagate upstream and interact with the vortical structures present in the wake of the above blade. Their presence within the flow is clear although these $S_i$ waves seem to be rapidly dissipated by the flow and the numerical model. The pressure side waves, $P_i$, also travel upstream but rapidly encounter the suction side wall of the neighboring blade located below. This interaction results in a reflected wave which eventually crosses the $P_{i+1}$ wave. Further increase in the numerical complexity and turbulent

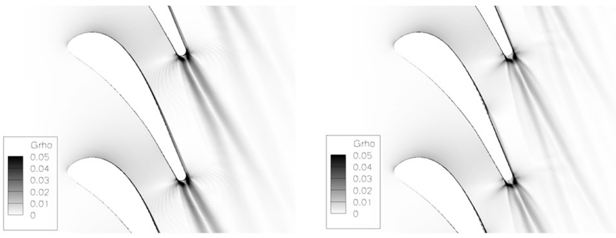


(*a*) (*b*)

**Fig. 6 Temporal mean solution as obtained by use of (*a*) URANS and (*b*) LES. Note that both results can be directly compared to Fig. 5(*a*).**

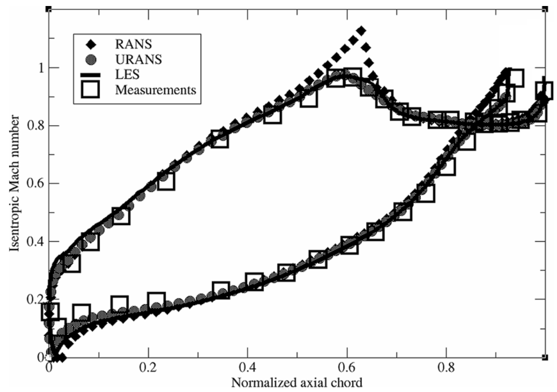


**Fig. 7 Mean isentropic Mach distribution along the blade wall predicted numerically and measured in the experiment**

modeling formulation (LES) provides an even finer view on the flow behavior (Fig. 5(*c*)). With LES, all flow structures identified by URANS are present: the vortex shedding from the blade leading edge, both sets of pressure waves and their propagation. The $P_i$ waves are also interacting with the main flow stream and impact the lower blade suction side wall. The main difference between URANS and LES appears on these instantaneous views to be highly local. The trailing edge sheds vortical structures that are more persistent in LES than in URANS producing more interactions between the wake and $S_i$ waves.

Differences in numerical formulations naturally induce different instantaneous views of the same problem as illustrated and discussed in Fig. 5. A more rigorous comparison of the two unsteady flow models that are URANS and LES requires a temporally averaged field comparison as provided in Fig. 6. Based on these mean fields, unsteady flow approaches predict similar flows which differ from the stationary approach predictions provided by RANS (Fig. 5(*a*)). Differences between mean flow fields obtained by URANS and LES are located in the wake region and the zone where wave propagation occurs. With LES, the mean wake has a larger opening angle than the one obtained by URANS which itself is larger than RANS. These subtle differences can be explained by the differences in models and formulations. Indeed when URANS relies on a statistically stationary representation of turbulence on the top of well defined flow oscillation frequencies, LES aims at providing a model for the turbulent scales filtered out by the mesh. In the first case, the entire range of turbulent scales are modeled including the large flow scales although they might be of a different nature and highly anisotropic. In the second case, the large scales are inherently present and only the ideally more isotropic and scale independent SGS field is modeled. The net result of such different formulations is in the case of URANS, a turbulence model that is potentially more dissipative/diffusive than the one offered by LES, as clearly visualized on the instantaneous views of Fig. 5.

**Table 3 Wake shedding frequency expressed in terms of Strouhal number**

| Experiment | URANS (error) | LES (error) |
|---|---|---|
| 0.219 | 0.276 (+26%) | 0.228 (+4%) |

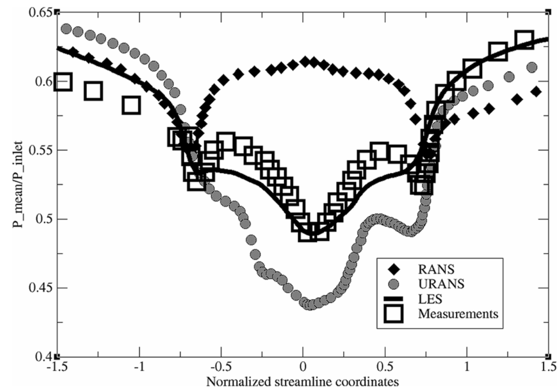


**Fig. 8 Mean pressure distribution along the blade trailing edge as predicted numerically and measured in the experiment**

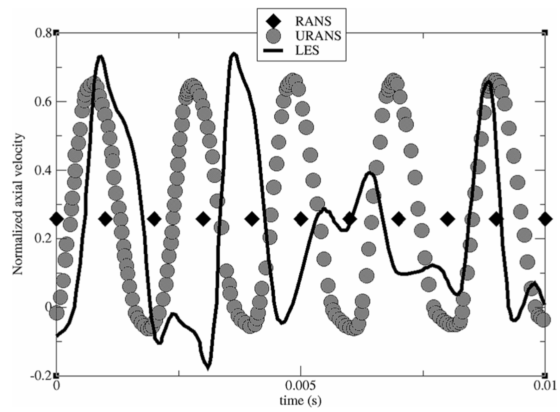


**Fig. 9 Temporal evolution of the axial velocity component in the wake of the blade**

An unambiguous validation of the mean flow predictions is obtained thanks to a direct comparison of the isentropic Mach distribution along the blade surface as predicted by the three numerical approaches and measured experimentally (Fig. 7). Again, going from a purely stationary numerical model to an unsteady model clearly improves the flow predictions. Hence and in agreement with the discussion started above, the RANS prediction leads to a local misrepresentation of the flow field. In particular, a passage shock ($M_{\mathrm{is}} > 1$) appears with RANS when it is not present in the experiment. URANS and LES allow net improvements when compared to RANS, with relatively small and only localized distinctions between the two unsteady flow approaches and for this blade quantity. Differentiation between URANS and LES is better indicated by purely unsteady flow phenomena such as the wake shedding frequency that is provided in Table 3 and is expressed in terms of Strouhal[4] number as defined by experimentalists [9,10]. Differences are also identified when looking at the trailing edge mean pressure field as shown in Fig. 8. For this specific region, only LES seems to recover the pressure level

[4]The spectral analysis relies on a time series of 3 ms obtained for a numerical and experimental probes located at $x/c_{\mathrm{ax}} = 0.933$ and pictured in Fig. 16(*g*). Note that this duration corresponds approximately to 20 cycles of the wake shedding.

measured experimentally, URANS offering an important alternative to RANS. The different levels of unsteadiness provided by the two unsteady flow approaches are illustrated in Fig. 9. In this figure, the axial velocity component of the velocity vector in the wake of the blade is given as a function of time. The point of interest is located at $0.5c_{ax}$ away from the blade in the wake direction. From this diagnostic, not only does the fluctuating component differ between URANS and LES but also the frequency content of both time series indicates one sole frequency in URANS and several for LES. More details on this specific flow response are provided afterwards in the context of the mesh LES sensitivity analysis.

Preliminary conclusions on the numerical formulation to be used to reproduce the turbulent flow encountered in a turbine blade at high subsonic outlet number are as follows. First, it seems important to be able to take into account the unsteady nature of the physics involved. This observation implicitly disqualifies the RANS approach although use of second order modeling strategies [25] may be of use (which is not the type of closure proposed here). Second, use of URANS offers a net improvement over RANS and again higher order closures seem recommended to better capture turbulence interactions. Finally, LES, which is a fully unsteady numerical approach, captures most of the physics reported by the experimentalists. Further investigations need however to be conducted as LES predictions are by construction mesh dependent as well as very sensitive to numerics and wall modeling. Preliminary insights on these issues are presented in the following where two fully compressible flow solvers are gauged on the previous test case.

## LES Sensitivity Analysis

LES relies on the notion of scale separation which is implicitly or explicitly introduced theoretically to derive the filtered fully compressible set of Navier–Stokes equations. In practice, the filter size is linked to the local cell volume of the mesh [6] which induces a numerical flow prediction dependency on that parameter. Numerical integration of the closed LES equations also influences the solution. Indeed, each scheme has specific dispersion/dissipation properties which will impact the propagation speeds and attenuation rates of the physical flow information across the computational domain. All these issues are well identified in the framework of LES [6,26] and can be partly reduced to the following problems:

- Numerics: temporal and spatial integration of the governing equations (implicit versus explicit schemes, upwind versus centered spatial discretization and orders of accuracy)
- Grid topology: fully structured, unstructured or hybrid meshes
- SGS modeling: filter size, wall resolution
- Computer architecture: round-off errors, parallelization

Identifying individual contributions of all these potential sources of errors and their propagation or contribution in a LES prediction is a very difficult goal due to the natural resonator/amplification behavior of the discrete system solved by the computer [27]. From a pragmatic point of view, part of the answer can be addressed by using two different codes on the same problem keeping as many parameters identical. For the problem considered here a block-structured cell-centered finite-volume LES code [28] is compared to a fully unstructured cell-vertex finite-volume LES code [29]. Both codes use no-slip wall conditions and the Smagorinsky SGS closure [21] with a constant set to 0.09 and no damping function. The characteristics of each code and models are detailed in Table 4 and this allows numerical strategies for turbine blade LES computations to be compared.

**Table 4 LES codes characteristics**

| Code | Temporal discretization | Spatial discretization |
|---|---|---|
| Structured finite-volume [30] | Implicit $O(\Delta t^2)$ | Centered $O(\Delta x^3)$ |
| Unstructured finite-volume [20] | Explicit $O(\Delta t^3)$ | Centered $O(\Delta x^3)$ |

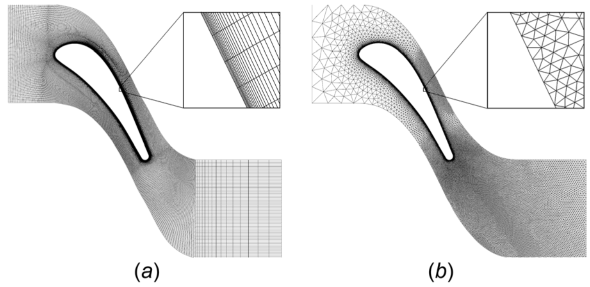


**Fig. 10 Mesh point distribution for the (*a*) structured and (*b*) unstructured meshes**

**Table 5 Grid parameters used for the LES sensitivity analysis**

| | Points | Cells | Mean $y^+$ | Geometry |
|---|---|---|---|---|
| Structured meshes | | | | |
| H1 | 97,000 | 62,000 | 12 | 3D |
| H2 | 636,000 | 500,000 | 5 | 3D |
| Unstructured meshes | | | | |
| T1 | 17,000 | 32,000 | 250 | 2D |
| T2 | 79,000 | 154,000 | 15 | 2D |
| T3 | 400,000 | 1,900,000 | 60 | 3D |

**Flow Solver Sensitivity Analysis.** With these two codes at hand, the impact of numerics, wall resolution and grid topology is specifically questioned and quantified in the context of the high subsonic Mach number turbine blade detailed above. For such an analysis, several grids are produced based on a given mesh topology taking advantage of each approach. Figure 10 presents the mesh refinement strategy adopted for each code. The list of mesh characteristics and typical mean $y^+$ associated with the first wall cells are given in Table 5.

The prime advantage of an implicit fully structured LES code resides in its ability to finely mesh the blade boundary layer without enforcing a very small time-step as needed by CFL stability criterion of explicit convection schemes. The disadvantage arises from the constraint of propagating the wall fine grid topology far into the computational domain. Explicit integration imposes stringent CFL conditions which are directly linked to the smallest cell size in the computational domain. The main consequence is that for the target application where the Reynolds number is very high, achieving a $y^+$ at the limit of the viscous sublayer is not possible since it implies too small time-steps. However, local grid refinement or coarsening within the flow is eased when compared to the structured implicit approach. Grid points can hence be concentrated in regions of interest where important unsteady flow features are expected as seen in Fig. 10.

Note that the first set of computations comparing RANS, URANS and LES predictions, were obtained with the block-structured LES code and were conducted taking the full three-dimensional computational domain with a spanwise dimension of 5.7% chord length to allow affordable and fast computations. Preliminary verification of the flow three-dimensionality confirmed that most of the information of interest is two-dimensional which is in agreement with the initial intent of the experimentalists [9,10]. For the current study which concentrates on LES and when

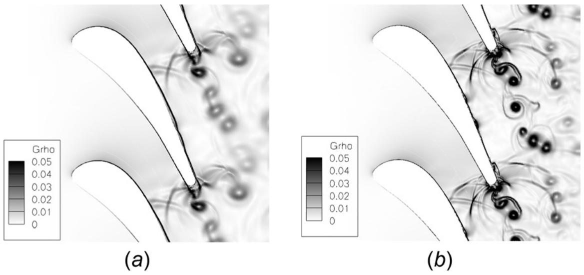


**Fig. 11 Typical snapshot of the density gradient obtained with the block-structured meshes: (*a*) H1 and (*b*) H2**

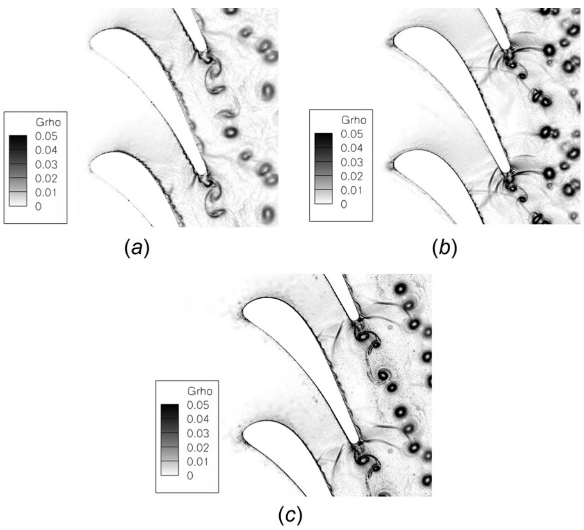


**Fig. 12 Typical snapshot of the density gradient obtained with the unstructured meshes: (*a*) T1, (*b*) T2, and (*c*) T3**

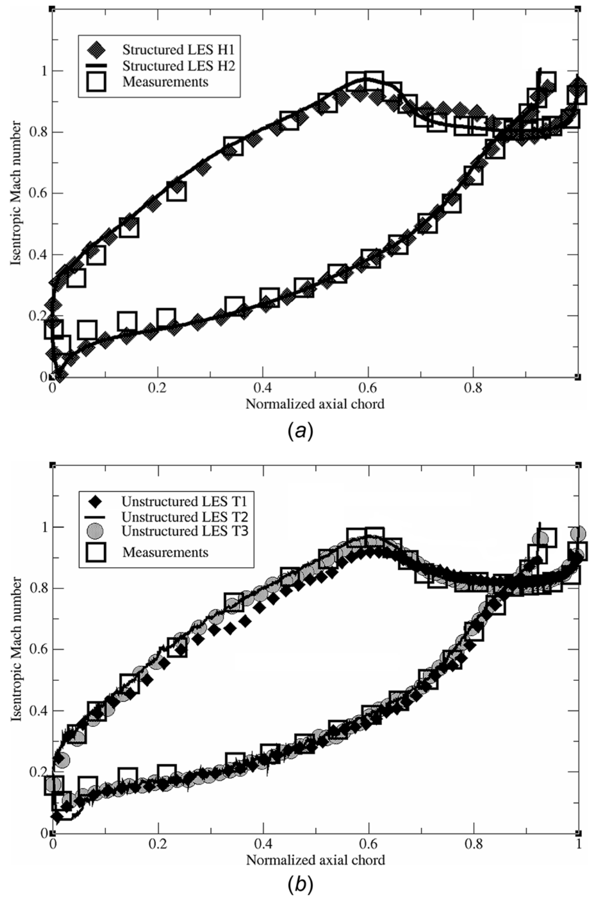


**Fig. 13 Mean isentropic Mach distribution along the blade wall and as a function of the mesh resolution: (*a*) structured and (*b*) unstructured meshes**

possible with the solver, 2D and 3D computational domains are considered without loss of generality, at least for most presented profiles. Further investigations are being pursued to fully assert the findings and extend the results to full 3D applications.

**Unsteady, Mean Flow Results, and Validation.** As discussed above, LES instantaneous solutions are inherently dependent on the local mesh resolution, although mean statistical independence of the first and second moments of the temporally averaged LES predictions can be expected. In the case of wall bounded flows, the grid dependency is even more important since part of the flow dynamics is issued by the boundary layer physics. Having access to an implicit code allows the wall region to be finely meshed without constraining the numerical time-step (Fig. 10(*a*)). The disadvantage is that wall cells are usually very stretched and this local mesh resolution extends far into regions of lesser interest. Going to the unstructured meshes offers greater flexibility. However, this code being explicit in time, the local cell size needs to be controlled to not yield too small a time-step for the simulation to be converged.

Effects of the wall mesh resolution, are illustrated in Fig. 11 for the structured code and Fig. 12 for the unstructured code. In such diagnostics, instantaneous views of the density gradient are provided for all the meshes. As a whole, all LES predictions recover the dynamics identified previously. The change of resolution and numerical scheme is essentially seen in the wake region where the vortical patterns differ slightly in their spatial organization. Such differences imply different wave patterns emitted from the trailing edge. As the mesh resolution is locally increased, such waves are more numerous and more localized as well as better defined irrespectively of the code used. Along the blade wall on the suction side, wall vortices are also present in all LES predictions. For the fully structured implicit approach, the near wall vortices are small and elongated when they appear larger and stronger with the unstructured explicit solver. For these structures, the local wall resolution seems to play a role at least when looking at instantaneous views of the predictions.

A better evaluation of the impact of the wall resolution on the LES predictions is obtained by comparing the mean isentropic Mach profile along the blade with experimental findings for the structured meshes (Fig. 13(*a*)) and the unstructured meshes (Fig. 13(*b*)). With the fully structured implicit code, the experimental profile is reasonably well recovered for all meshes although clear improvement could be obtained but with a non-negligible increase of resolution and computer cost. For information, the computer effort needed for the current simulations[5] is provided in Table. 6. Such numbers and boundary layer profiles underline the difficulty encountered by LES at walls even for fully structured implicit solvers. Note also that the mesh resolution along the wall and in the main channel is also found to impact the suction side region located behind the high isentropic Mach value of $\approx 0.95$. In this zone which corresponds to the impact of the $P_i$ waves, a plateau appears followed by a sudden drop of the isentropic Mach curve if the grid resolution is not adequate. The presence of the plateau was identified as coming from the SGS model and grid local resolution which result in a locally artificially thickened boundary layer. Such a model response is reduced by

[5]Corresponding to a converged simulation for RANS and a temporal integration of 10 ms for LES (note that around 40 ms are needed to pass the transient phase).

**Table 6 Computer costs issued by the different approaches and meshes**

| | Mesh | CPU (h) | Elapsed time (h) | Processor number |
|---|---|---|---|---|
| RANS | H2 | 30 | 2.5 | 12 |
| URANS | H2 | 336 | 28 | 12 |
| LES | H1 | 20.5 | 1.3 | 16 |
| | H2 | 267 | 16.7 | 16 |
| | T1 | 2 | 0.1 | 32 |
| | T2 | 73.2 | 2.3 | 32 |
| | T3 | 950 | 23.8 | 40 |

increasing the local mesh resolution or by changing the SGS model. Unstructured mesh predictions confirm the importance of the wall treatment and local mesh resolution. Indeed, predictions with $T1$ mesh (Table 5) do not fully predict the isentropic Mach profile on the suction side of the blade and only $T2$ or $T3$ meshes provide good quality profiles as reported in the experiment. Note however that with the unstructured code, the generated meshes allow a local refinement of $P_i$ waves' impact region as well as the channel resolution directly above this specific region. The main outcome is an improved flow prediction in this specific area (when compared to the coarse structured code predictions) even for a reduced number of grid nodes.

A more local comparison of the two LES numerical approaches are presented in Fig. 14. In this analysis, the boundary layer profiles at two stations (Fig. 1(*b*)) are compared to experimental measurements. Use of a fine mesh in the wall region is here clear (Figs. 14(*a*) and 14(*b*)) and having access to a fully implicit structured code offers enough flexibility to improve this flow region without implying intractable time-stepping. Use of an explicit unstructured code (Figs. 14(*c*) and 14(*d*)) implies a clear sacrifice in the flow description within the boundary layer. This issue is more critical on the suction side of the blade. In all cases, it is also clear from such diagnostics that the numerical profiles provide boundary layer profiles that point to lower effective wall Reynolds number flows than in the experiment. This issue of effective versus real flow Reynolds number is critical especially for real applications with much higher values and geometrical complexity. It is still not clear which numerical approach is better suited and this analysis only highlights the difficulties in performing LES of such flows. Alternatives for the LES wall treatment are possible and among other solutions the law-of-the-wall modeling, Detached Eddy Simulation (DES) [31,32] or multiscale modeling approaches are good candidates. Such alternatives are however outside the scope of this work and would necessitate detailed validations and developments prior to their application to real applications.

Preliminary LES instantaneous snapshots point to the trailing edge flow region as being critical in the determination of the unsteady flow features. In particular, the waves generated in this zone seem to be of importance since they interact with the suction side of the neighboring blade and can interact with the neighboring wakes. Mean pressure profiles along the curvilinear coordinate

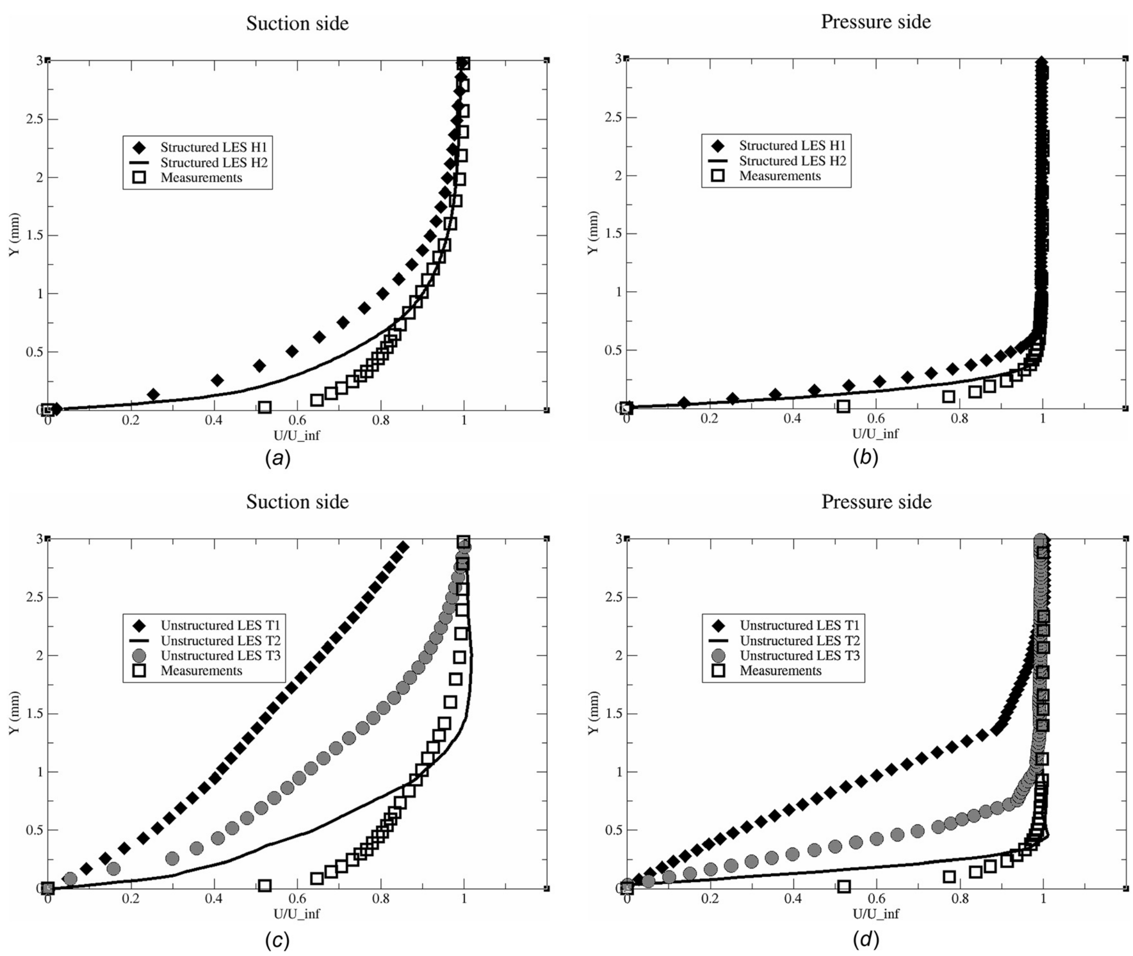


**Fig. 14 Mean boundary layer profiles as a function of the mesh resolution: (*a*) and (*b*) structured and (*c*) and (*d*) unstructured meshes. The two sides of the blade are presented: (*a*) and (*c*) for the suction side and (*b*) and (*d*) for the pressure side.**

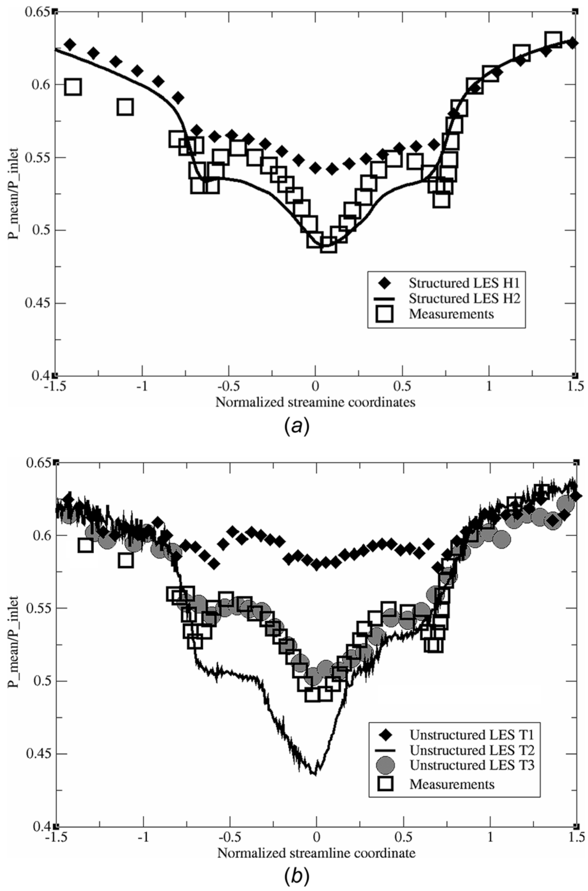


**Fig. 15 Mean trailing edge pressure profile as a function of the mesh resolution: (*a*) structured and (*b*) unstructured meshes**

of the trailing edge indicate the sensitivity of the trailing edge region to the mesh resolution and results are given in Fig. 15. Here again and in agreement with the previous findings, the wall resolution is of importance and only well refined meshes guarantee proper estimations of the experimental measurements. In this region, none of the LES predictions is satisfactory. However, if the wall region is appropriately modeled, all LESs will produce better quality pressure profiles than the other two numerical approaches. It is also worth mentioning that going from 2D to full 3D LES seems to be a prerequisite if that specific profile is to be well reproduced numerically. Indeed, although $T3$ wall resolution may not be adequate in part of the blade boundary layer, the conjunction of local mesh refinement and three-dimensionality at the trailing edge seems to be sufficient to provide interesting results in good agreement with the experiment. Of course such observations highlight again the difficulty of performing high quality LES modeling of such flows. Current investigations on the effect of the local resolution as well as the importance of the spanwise extend of the computational domain on the LES predictions are being pursued.

Despite this shortcoming and the potential limitations of the LES predictions at given flow stations, a comparison is proposed for unsteady quantities. Indeed, unsteady experimental measurements of pressure fluctuations at specific blade stations and a direct comparison of LES and experiment is presented in Fig. 16. For clarity and based on the previous analyses of the LES predictions, only $H2$ and $T3$ are gauged against the experiment. From Fig. 16, it is clear that not only are the two codes able to quantify the pressure variations within the flow, but they are also able to recover the spatial evolution of these oscillations. The mechanism yielding to the wave generation and located at the trailing edge is properly reproduced with $H2$ and $T3$. This conclusion is valid only if the mean trailing edge pressure profile is properly approximated: i.e., RANS and URANS do not produce comparable predictions even if URANS clearly outperforms RANS. With both LES codes, the mean trailing edge pressure oscillation at stations 5 and 6, Figs. 16(*e*) and 16(*f*) are very well estimated. The frequency of the boundary layer detachment point on the suction and pressure sides is captured. The amplitude of the phenomenon could be improved especially on the suction side. However, this specific criterion needs to be investigated more to remove potential low frequency phenomena that are not adequately addressed for the time duration under consideration. Propagation of the $P_i$ waves upstream and downstream the blade passage yields to a natural attenuation of the transmitted information until it eventually hits the lower blade suction side wall as illustrated in Figs. 11 and 12. In the downstream wave propagation region, station 4, the local pressure signal as provided by LES is composed of different features. The main frequency corresponds to the frequency of the wave issued by the above blade trailing edge. A second contribution may be identified and linked to potential trace of the wall vortices whose frequency depends on the simulation. Despite these complex dynamics, both codes seem able to at least recover the mean pressure signal variation and its peak amplitude in the entire downstream part of the blade passage. Going upstream along the blade suction side wall, in the vicinity of the wave impact point, the pressure signal registered in the experiment and in LES changes in shape. All downstream points recorded time series are near sinusoidal in shape. In the region of impact where the waves issued by the trailing edge travel upstream, the initially sinusoidal shape straightens out to produce a sawtooth signal at station 3 with highly pronounced pressure jumps. Here again both codes are able to at least recover the change in shape although there still exists room for improvement. Upstream of station 3, points 2 and 1 have strongly attenuated pressure oscillations up to point where no wave is measured experimentally or observed numerically: i.e., no more upstream propagation of the waves.

All of these advanced and unsteady confrontations between different LES codes and measurements confirm the overall potential of LES and clearly opens interesting perspectives.

## Conclusion

Comparisons of the RANS, URANS, and LES numerical procedures for a well-documented turbine blade experiment of Sieverding et al. [9,10] confirm the potential of the fully unsteady flow approach that is LES. Although RANS offers good estimates of the mean flow quantities (isentropic Mach number and boundary layer thickness at two stations on the blade), LES and URANS are the only approaches that can produce the proper trailing edge flow dynamics. However, only LES seems to offer a complete view of the complex flow. Indeed, LES identifies most flow phenomena in agreement with the experiment. For example, sound waves emitted from the trailing edge boundary layer separation point propagate upstream and interact with the lower blade suction side to generate small vortices propagating downstream.

To further investigate the LES approach, comparisons and grid dependencies of the results are then presented for fully structured implicit and unstructured explicit simulations. That sensitivity analysis, although not fully comprehensive in terms of the different sources of errors issued by LES, confirms a few important observations. In particular, the wall resolution and modeling needed to offer a good quality LES flow description of all the various phenomena (i.e., boundary layers, wake shedding and the pressure wave generation) is of importance irrespectively of the numerical approach and grid topology. This observation has important consequences in the context of LES of real applications. Further investigations are needed, however, to fully assess the use of LES for such flows. In particular, the need for adequate wall treatments remains to be evaluated if real industrial turbine flows

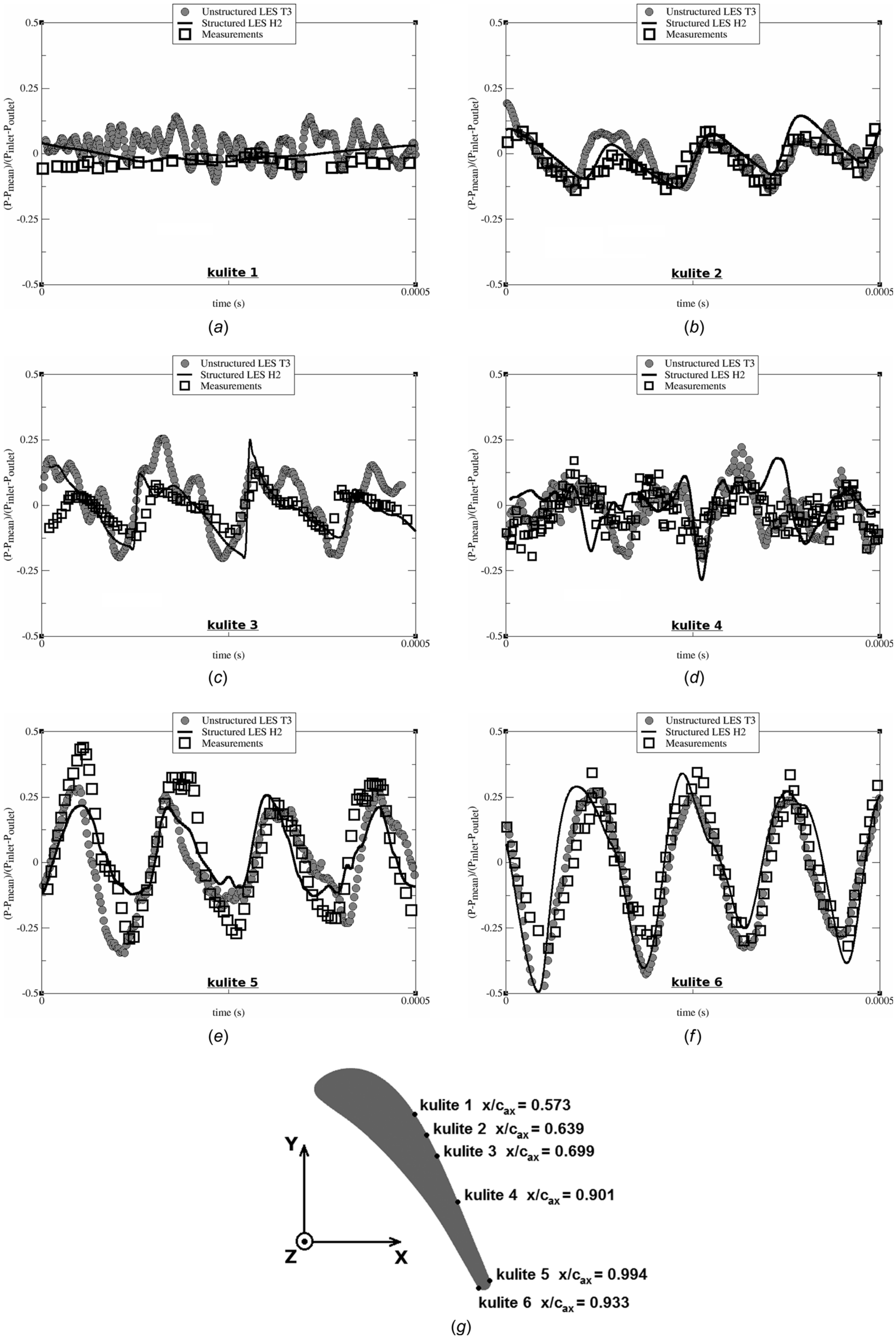


**Fig. 16 Unsteady pressure signal comparisons as issued by structured and unstructured LES at positions along the blade wall**

are to be investigated by LES. Likewise, the computational cost and prediction sensitivity to the spanwise length of the computational domain are still to be investigated. Despite these findings and with the computational constraints devised in this work, the unsteady nature of LES predictions is very encouraging and experimental unsteady features are well captured by both codes. It clearly opens new perspectives for LES to contribute in the understanding of such turbine blade flows.

## Acknowledgment

Thanks go to T. Arts from VKI for suggesting the test configuration. The work presented here was possible thanks to access to the CERFACS internal computing facility as well as access to the CINES (Centre Informatique National de l'Enseignement Supérieur) located in Montpellier, France under the project fac6074.

## Nomenclature

$c$ = speed of sound
is = isentropic value
$M$ = Mach number
$P$ = pressure
Re = Reynolds number
$T$ = temperature
$U$ = axial velocity component
$V$ = transverse velocity component
$W$ = spanwise velocity component
$\rho$ = density
0 = inlet value
2 = outlet value
$^+$ = wall unit

## References


[1] Wilcox, D., 1995, *Turbulence Modeling for CFD*, DCW Industries, La Cañada, CA.
[2] Anderson, J. D., 1995, *Computational Fluid Dynamics*, McGraw-Hill, New York.
[3] Tennekes, H., and Lumley, J. L., 1972, *A First Course in Turbulence*, MIT, Cambridge, MA.
[4] Lardeau, S., and Leschziner, M., 2004, "Unsteady Reynolds-Averaged Navier–Stokes Computations of Transitional Wake/Blade Interaction," AIAA J., **42**(8), pp. 1559–1571.
[5] Ferziger, J. H., and Perić, M., 1997, *Computational Methods for Fluid Dynamics*, Springer-Verlag, Berlin.
[6] Sagaut, P., 2000, *Large Eddy Simulation for Incompressible Flows* (Scientific Computation Series), Springer-Verlag, Heidelberg, Germany.
[7] Cebeci, T., and Cousteix, J., 2005, *Modeling and Computation of Boundary-Layer Flows*, Springer and Horizons, Berlin.
[8] Piomelli, U., 2008, "Wall-Layer Models for Large-Eddy Simulations," Prog. Aerospace Sci., **44**(6), pp. 437–446.
[9] Sieverding, C., Richard, H., and Desse, J.-M., 2003, "Turbine Blade Trailing Edge Flow Characteristics at High Subsonic Outlet Mach Number," ASME J. Turbomach., **125**(2), pp. 298–309.
[10] Sieverding, C., Ottolia, D., Bagnera, C., Comadoro, A., Brouckaert, J.-F., and Desse, J.-M., 2004, "Unsteady Turbine Blade Wake Characteristics," ASME J. Turbomach., **126**(4), pp. 551–559.
[11] Pope, S. B., 2000, *Turbulent Flows*, Cambridge University Press, Cambridge, UK.
[12] Hirsch, C., 1988, *Numerical Computation of Internal and External Flows*, Vol. 1, Wiley, New York.
[13] Gourdain, N., Gicquel, L., Montagnac, M., Vermorel, O., Gazaix, M., Staffelbach, G., Garcia, M., Boussuge, J.-F., and Poinsot, T., 2009, "High Performance Parallel Computing of Flows in Complex Geometries: I. Methods," J. Comput. Sci. Discovery, **2**(1), p. 015003.
[14] Gourdain, N., Gicquel, L., Staffelbach, G., Vermorel, O., Duchaine, F., Boussuge, J.-F., and Poinsot, T., 2009, "High Performance Parallel Computing of Flows in Complex Geometries: II. Applications," J. Comput. Sci. Discovery, **2**(1), p. 015004.
[15] Shang, T., and Epstein, A., 1997, "Analysis of Hot Streak Effects on Turbine Rotor Heat Load," ASME J. Turbomach., **119**(3), pp. 544–553.
[16] Cutrone, L., De Palma, P., Pascazio, G., and Napolitano, M., 2005, "Assessment of Laminar-Turbulent Transition Models for Turbomachinery Flow Computations," ASME Paper No. GT2005-68330.
[17] Wilcox, D., 1988, "Reassessment of the Scale-Determining Equation for Advanced Turbulence Models," AIAA J., **26**(11), pp. 1299–1310.
[18] Zheng, X., and Liu, F., 1995, "Staggered Upwind Method for Solving Navier–Stokes and $k-\omega$ Turbulence Model Equations," AIAA J., **33**(6), pp. 991–998.
[19] Jameson, A., 1991, "Time Dependent Calculations Using Multigrid, With Applications to Unsteady Flows Past Airfoils and Wings," AIAA Paper No. 91-1596.
[20] Colin, O., and Rudgyard, M., 2000, "Development of High-Order Taylor-Galerkin Schemes for Unsteady Calculations," J. Comput. Phys., **162**(2), pp. 338–371.
[21] Smagorinsky, J., 1963, "General Circulation Experiments With the Primitive Equations: 1. The Basic Experiment," Mon. Weather Rev., **91**(3), pp. 99–164.
[22] Deardorff, J. W., 1970, "A Numerical Study of Three-Dimensional Turbulent Channel Flow at Large Reynolds Numbers," J. Fluid Mech., **41**(2), pp. 453–465.
[23] Meneveau, C., 1994, "Statistics of Turbulence Subgrid-Scale Stresses: Necessary Conditions and Experimental Tests," Phys. Fluids, **6**(2), pp. 815–833.
[24] O Neil, J., and Meneveau, C., 1997, "Subgrid-Scale Stresses and Their Modelling in a Turbulent Plane Wake," J. Fluid Mech., **349**, pp. 253–293.
[25] Launder, B., Reece, G., and Rodi, W., 1975, "Progress in the Development of a Reynolds-Stress Turbulent Closure," J. Fluid Mech., **68**(3), pp. 537–566.
[26] Ghosal, S., and Moin, P., 1995, "The Basic Equations for the Large Eddy Simulation of Turbulent Flows in Complex Geometry," J. Comput. Phys., **118**(1), pp. 24–37.
[27] Senoner, J.-M., García, M., Mendez, S., Staffelbach, G., Vermorel, O., and Poinsot, T., 2008, "The Growth of Rounding Errors and the Repetitivity of Large Eddy Simulation on Parallel Machines," AIAA J., **46**(7), pp. 1773–1781.
[28] Cambier, L., and Veuillot, J.-P., 2008, "Status of the *els*A CFD Software for Flow Simulation and Multidisciplinary Applications," AIAA Paper No. 2008-664.
[29] Garcia, M., 2009, "Développement et validation du formalisme euler-lagrange dans un solveur parallèle et non-structuré pour la simulation aux grandes échelles," Ph.D. thesis, Université Paul Sabatier, Toulouse.
[30] Liou, M. S., 1996, "A Sequel to AUSM: AUSM$^+$," J. Comput. Phys., **129**, pp. 364–382.
[31] Spalart, P. R., Jou, W.-H., Stretlets, M., and Allmaras, S. R., 1997, "Comment on the Feasibility of LES for Wings and on the Hybrid RANS/LES Approach, Advances in DNS/LES," 1st AFOSR International Conference on DNS/LES, Louisiana Tech University, Ruston, LA.
[32] Deck, S., 2005, "Numerical Simulation of Transonic Buffet Over a Supercritical Airfoil," AIAA J., **43**(7), pp. 1556–1566.